



## Preparation and Properties of Sodium Alginate/ Gelatin Hydrogel-Microspheres

Wen-jie Tang, Jin-xin Zhang, Liang Liu, Lu-yao Zhao, Liu Wang, Chang Shi,  
Yang Liu & Mei-ling Wen

To cite this article: Wen-jie Tang, Jin-xin Zhang, Liang Liu, Lu-yao Zhao, Liu Wang, Chang Shi, Yang Liu & Mei-ling Wen (2024) Preparation and Properties of Sodium Alginate/Gelatin Hydrogel-Microspheres, Journal of Macromolecular Science, Part B, 63:3, 146-160, DOI: [10.1080/00222348.2023.2254578](https://doi.org/10.1080/00222348.2023.2254578)

To link to this article: <https://doi.org/10.1080/00222348.2023.2254578>



Published online: 13 Sep 2023.



Submit your article to this journal [↗](#)



Article views: 276



View related articles [↗](#)



View Crossmark data [↗](#)



# Preparation and Properties of Sodium Alginate/Gelatin Hydrogel-Microspheres

Wen-jie Tang<sup>a,b\*</sup>, Jin-xin Zhang<sup>c\*</sup>, Liang Liu<sup>d</sup>, Lu-yao Zhao<sup>a,b</sup>, Liu Wang<sup>a,b</sup>,  
Chang Shi<sup>e</sup>, Yang Liu<sup>a,b,f</sup>, and Mei-ling Wen<sup>a,b</sup>

<sup>a</sup>Institute of Biomedical Engineering, College of Biomedical Engineering, Taiyuan University of Technology, Shanxi Key Laboratory of Material Strength & Structural Impact, Taiyuan, Shanxi, China; <sup>b</sup>Research Center for Nanobiomaterials & Regenerative Medicine, College of Biomedical Engineering, Taiyuan University of Technology, Taiyuan, Shanxi, China; <sup>c</sup>College of Life, Northwestern Polytechnical University, Xian, Shanxi, China; <sup>d</sup>Jilin Aile New Technology Co., Ltd, Changchun, Jilin, China; <sup>e</sup>Sale & Marketing Manger, IVD, Mindray Medical International Ltd, Taiyuan, Shanxi, China; <sup>f</sup>Department of Nuclear Medicine, First Hospital of Shanxi Medical University, Taiyuan, Shanxi, China

## ABSTRACT

Calcium alginate gel microspheres exhibiting pH response release characteristics were prepared, and utilizing Bovine serum albumin (BSA) to evaluate drug release performance. Hydrogels composed of gelatin (GL) and sodium alginate oxide (NALO), with varying ratios (7:3; 4:1; 3:2) were prepared by controlling their composition. Scanning electron microscopy (SEM) and a microplate reader (ELIASA) were used to characterize the microspheres' microstructure and *in vitro* BSA release behavior, respectively. The results demonstrated that, under acidic conditions, the BSA release was slower than in neutral conditions. The hydrogels' physical and chemical properties were analyzed using optical microscopy, Fourier transform infrared spectroscopy (FTIR), swelling experiments and mechanical testing of the hydrogels and microsphere loaded hydrogels. The results showed that a GL to NALO ratio of 7:3 increased the swelling degree, while a 4:1 ratio optimized the mechanical characteristics. The study concluded that the microsphere-loaded hydrogels exhibited significant potential for human drug delivery applications.

## ARTICLE HISTORY

Received 26 July 2023  
Accepted 29 August 2023

## KEYWORDS

Drug delivery systems;  
hydrogels; microspheres;  
skin dressing

## 1. Introduction

Addressing the challenges of controlling wound healing remains a pressing clinical dilemma. The inability to effectively manage this process not only places immense strain on patients' physical and psychological well-being but also amplifies the burden of social medical resources.<sup>[1]</sup> Among the strategies to mitigate this issue, skin dressings have been shown to expedite wound healing. Particularly, hydrogel-based wound dressings have emerged as a promising solution. Comprised of hydrophilic polymers characterized by high water content, swelling, insolubility and a three-dimensional cross-linked network structure,<sup>[2]</sup> these hydrogels are regarded by both medical professionals and academic researchers as the synthetic material most akin to human soft tissue.<sup>[3]</sup>

**CONTACT** Dr. Yang Liu [liu\\_yang\\_tai\\_yuan@163.com](mailto:liu_yang_tai_yuan@163.com); Dr. Mei-ling Wen [wenmeiling@tyut.edu.cn](mailto:wenmeiling@tyut.edu.cn) College of Biomedical Engineering, Taiyuan University of Technology, Jinzhong City, Shanxi Province, China.

\*Wen-jie Tang and Jin-xin Zhang contributed equally to this study.

Due to the complexity of the human skin microenvironment, the design and formulation of superior skin dressings require a meticulous approach. It is imperative that they harmonize with the skin's pH, acknowledging the pathological nuances and structural features of an inflamed site.<sup>[4]</sup> Beyond these physiological considerations, the chosen dressing material must also meet essential criteria of safety, cost-effectiveness and biocompatibility to ensure therapeutic success and patient well-being.<sup>[5,6]</sup> Hydrogel BSA-loading systems, in this context, are noteworthy for their commendable biocompatibility, controllable degradation profiles and inherent drug protection functions.<sup>[7]</sup> The porous structure of these hydrogels plays a pivotal role in facilitating the encapsulation and transport of a diverse range of protein and peptide therapeutics. This spectrum includes enzymes, albumin, biological hormones and small molecule fragments derived from body fluids like blood and lymph.<sup>[8,9]</sup> Such attributes position hydrogels as promising drug delivery vectors. Recent advancements highlight the incorporation of peptide within these BSA-loaded hydrogel matrices, paving the way for innovative wound repair applications.<sup>[10,11]</sup>

Sodium alginate, a natural polysaccharide, is composed of  $\beta$ -1,4-D mannuronic acid and  $\alpha$ -1,4-D guluronic acid moieties.<sup>[12,13]</sup> Praised for its biocompatibility and film-forming capabilities, it is not without challenges to use, such as excessive viscosity, resistance to injection and unexplained mucosal contraction.<sup>[14]</sup> These phenomena can be attributed to the absence of cationic components within the natural form of sodium alginate<sup>[15]</sup> and the instability of its viscosity when interacting with the multifarious environments of the digestive tract.<sup>[16,17]</sup> However, the advent of oxidative modification through sodium periodate has introduced an avenue for enhancement. The vicinal diol-OH groups within sodium alginate undergo chain scission to form aldehyde groups (-CHO), which can be coupled with gelatin, remediating the above limitations of sodium alginate.

Gelatin, a macromolecular protein derived from collagen through moderate degradation or thermal denaturation, is distinguished by its low antigenicity, macrophage activation and hemostatic properties.<sup>[18]</sup> By forestalling wounds infection, gelatin contributes to the expedited healing process, establishing itself as an ideal constituent for wound dressing materials. Its applications span from wound dressings and hemostatic agents to artificial skin constructs. Choi et al.<sup>[19]</sup> have demonstrated the successful integration of gelatin with sodium alginate to fabricate a composite sponge, further augmented with silver sulfadiazine, for effective repair of dorsal skin injury in rats. The resultant gelatin-sodium alginate composite sponge manifested an enhanced capacity for wound healing. However, the application of gelatin presents certain challenges, including its susceptibility to dissolution in water and instability within the physiological environment of the human body. Its degradation and metabolism in body fluids limit its standalone efficacy.<sup>[20]</sup>

In this study the prepared calcium alginate microspheres and gelatin-oxidized sodium alginate hydrogels underwent comprehensive characterization, employing techniques such as scanning electron microscopy (SEM), Fourier-transform infrared spectroscopy (FTIR) and swelling property assessments. The BSA release behavior of the microspheres was meticulously analyzed, shedding light on their pH-responsive BSA release properties. This study further explored the potential of GL/NALO-based hydrogels as viable candidates for BSA-loaded, sustained release skin dressings, paving the way for novel therapeutic interventions in wound management.<sup>[21,22]</sup>

## 2. Experimental

### 2.1. Materials

Sodium alginate was sourced from Tianjin Damao Chemical Reagent Factory (China), and anhydrous calcium chloride was procured from Tianjin Fengchuan Chemical Reagent Technology Co., Ltd. (China). Bovine serum albumin (BSA) was supplied by Beijing Solarbio Technology Co., Ltd. (China). Additional reagents, such as glacial acetic acid, hydroxylamine hydrochloride, methyl orange, and sodium citrate, were also obtained from Tianjin Fengchuan. 0.9% saline solution was sourced from Shijiazhuang Four Medicine Co., Ltd. (China), and phosphate buffered saline was purchased from Boster Bioengineering Co., Ltd. (China). Gelatin was acquired from Shanghai Yuanye Bio-Technology Co., Ltd. (China) and potassium periodate and ethylene glycol were obtained from Shanghai Aladdin Biochemical Technology Co., Ltd. (China). Sodium hydroxide (granular) was provided by Tianjin Hengxing Reagent Co., Ltd. (China).

### 2.2. Assembly of high-voltage electrostatic spray equipment

The high-voltage electrostatic spraying equipment was meticulously assembled to facilitate the preparation of the microspheres. Within the system, the positive pole of the high-voltage DC power supply was connected by a wire to the metallic segment of a copper clamp, thereby serving as the electrostatic spraying equipment's positive pole. Conversely, the negative pole of the high-voltage DC power supply was connected to a copper ring by a wire, designating it as the negative pole of the system. To ensure safety, insulation was used so that the components holding the copper clamps and rings remained non-conductive. The process for achieving smaller diameter microspheres entailed a series of connections: first, a syringe was connected to a 23 G Stainless Steel Dispensing Needle, followed by affixing the same needle to one end of Tygon tubing (model CN06419-01). Subsequently, the opposite end of the tubing was attached to a 30 G Medical Syringe Needle, which was then clamped with a copper clip. With all components securely fastened, the microsphere device was fully assembled and ready for operation.

### 2.3. Preparation of the calcium alginate microspheres

Sodium alginate was dissolved in double-distilled water, stirred using a magnetic stirrer for 1 h until fully dissolved, to prepare a 2% (w/v) sodium alginate (SA) solution. Solid  $\text{CaCl}_2$  was dissolved in distilled water, subsequently filtered to create a 4% (w/v)  $\text{CaCl}_2$  solution. In the preparation of the mixed solution, 0.25 g of BSA was added into 10 mL of the 2% (w/v) SA solution. It was stirred until dissolved and then heated in a water bath at 37 °C for 10 min to eliminate air bubbles, resulting in a homogeneous SA/BSA mixture. Carefully, 2 mL of the SA/BSA mixture was extracted by a syringe and injected at a uniform speed into 6 mL of the 4% (w/v)  $\text{CaCl}_2$  solution using a 30 G medical injection needle. During the injection the syringe needle was maintained at a distance of 10 cm from the liquid surface, and the injection speed was regulated at 5 mm/h. The mixed solution was stirred consistently at 300 r/min for 2 h to enable the cross-linking of the sodium alginate by the calcium ions. Following the completion of the reaction,

the residual solution was filtered, and the resulting product was washed with 0.9% saline, then dried to yield the desired microspheres.<sup>[23]</sup>

## 2.4. Characterization of the calcium alginate microspheres

### 2.4.1. SEM analysis

Upon completion of the fabrication process, the microspheres were subjected to vacuum freeze-drying at a temperature of  $-80^{\circ}\text{C}$ , meticulously preparing them for the subsequent phase of analysis. To enhance their conductive properties for observation, a delicate thin layer of gold was uniformly coated on the microspheres through a sputtering process (15 mA, 2 min). Utilizing the advanced capabilities of SEM and under the accelerating voltage of 5 kV, the apparent morphology of the microspheres was observed and photographed.

### 2.4.2. In-vitro BSA release test

To closely emulate the multifaceted physiological environment of the human body, an array of buffers were scrupulously prepared to mimic different pH conditions, including pH = 4.5 (concocted with glacial acetic acid and distilled water), pH = 7.25 (prepared using phosphate-buffered saline (PBS) buffer), and pH = 8.45 (composed with a 0.03 g/mL sodium citrate solution). Subsequently, 3 mg of the desiccated BSA-loaded microspheres were placed into 1 mL of the respective buffer solutions, which were then oscillated at a temperature of  $37^{\circ}\text{C}$ . Systematic sampling was conducted at regular intervals of 0.5 h, 1 h, and 3 h. During each sampling a quantitative amount of the buffer solution was extracted, with fresh buffer solution replenishing it to maintain a consistent 1 mL volume. Utilizing an enzyme labeling instrument, the absorbances of a pre-determined series of BSA concentrations at 280 nm were meticulously measured. This data enabled the construction of a standard curve, through which a linear regression equation was established. The absorbance of each group of BSA-loaded microspheres dissolved in the abovementioned buffers were then ascertained, allowing the calculation of the BSA concentration in the buffer of each group.<sup>[24]</sup> Subsequent calculations yielded the BSA loading and entrapment efficiency for each group of microsphere, achieved through the application of the following equations.

$$DL = \left( \frac{W_D}{W_P} \right) \times 100\% \quad (1)$$

$$EE = \left( \frac{DL \times W_P}{W_S} \right) \times 100\% \quad (2)$$

where  $DL$  is the BSA loading degree,  $W_D$  is the mass of the BSA in the microspheres,  $W_P$  is the mass of the microspheres,  $EE$  is the entrapment efficiency, and  $W_S$  is the total mass of BSA added.

## 2.5. Preparation of gelatin/oxidized sodium alginate (GL/NALO) hydrogels

1.5 g of sodium alginate was dissolved in 75 mL of deionized water, forming a 2% (w/v) sodium alginate solution. Separately, 0.75 g of sodium periodate was dissolved in 5 mL

of deionized water and this was added dropwise to the sodium alginate solution at room temperature. The mixture was stirred continuously for 24 h, and the complete oxidation reaction was carried out in the absence of light, forming the NALO. After this 24 h period, 1 mL of ethylene glycol was added to the mixture to terminate the oxidation process, with stirring continued at room temperature for an additional 2 h. The reaction solution was subsequently dialyzed with deionized water for 3 d and then freeze-dried to obtain solid NALO, stored at room temperature for future use.<sup>[25–27]</sup> When needed, three masses of solid NALO (0.08 mg, 0.06 mg, 0.04 mg) were dissolved in 2 mL of deionized water to form three different concentrations of NALO solutions (4%, 3%, 2% w/v). This was then mixed with 2 mL of gelatin solution in mass ratios of 3:2, 7:3, and 4:1 to prepare GL/NALO hydrogels, designated as G30NALO20, G35NALO15, and G40NALO10, respectively.

## **2.6. Preparation of microsphere-loaded hydrogels**

The GL/NALO hydrogels obtained, specifically G30NALO20, G35NALO15, and G40NALO10, were then mixed with 2 mg of core microspheres to obtain three distinct microsphere-loaded hydrogel formulations. These were designated as ZG30NALO20, ZG35NALO15, and ZG40NALO10, respectively.<sup>[28–30]</sup>

## **2.7. Characterization of hydrogels**

### **2.7.1. Assay for gel formation time of GL/NALO hydrogel**

In the experimental procedure the gelatin solution was combined with the oxidized sodium alginate solution within a glass container. During the cross-linking process, chemical bonds formed between the gelatin and NALO. The flow characteristics of the hydrogel were observed by inverting the container totally at an angle, with careful attention paid to the moment when the flow ceased. This point in time was recorded as the gelation time.<sup>[31]</sup>

### **2.7.2. FTIR spectroscopy of GL/NALO hydrogels**

The analysis of the samples through FTIR was carried out utilizing KBr pellets, employing a sophisticated Bruker Vertex 70 instrument (Bruker Alpha II, Bruker Co., Ltd., Germany). This instrumental technique facilitated the recording of FTIR spectra over a methodically selected wavelength range spanning from  $400\text{ cm}^{-1}$  to  $4000\text{ cm}^{-1}$ , with a resolution of  $4\text{ cm}^{-1}$ .

### **2.7.3. The swelling behavior of the GL/NALO hydrogels**

The samples of the hydrogels, representing different ratios, were selected and positioned within Petri dishes for analysis. The samples were subjected to freezing at a temperature of  $-20^\circ\text{C}$  for 2 h, followed by lyophilization at a temperature of  $-80^\circ\text{C}$  for an additional 6 h. The hydrogels were weighed utilizing a finely calibrated electronic balance to ascertain their dry weight. Subsequently, the aforementioned dried hydrogels were immersed in a phosphate buffers (PBS) solution, and then the hydrogel was removed

from the PBS solution at 1 min intervals and excess surface water was eliminated by blotting with filter paper. The mass of the gel was weighed again with the electronic balance. This operation was repeated until the gel weight no longer exhibited significant changes, signifying the swelling equilibrium attainment. The swelling ratio at each time point was calculated, applying the equation delineated as follows:

$$\text{Swelling Ratio} = \left( \frac{W_0 - W_n}{W_n} \right) \times 100\% \quad (3)$$

where  $W_n$  and  $W_0$  are the dry weight of the gel and the weight after water absorption at various times, respectively.<sup>[32]</sup>

#### **2.7.4. Determination of the loading rate of the microspheres in the GL/NALO hydrogels**

The mass of the microspheres, post freeze-drying, that was incorporated into the mixture of gelatin and NALO of each group was recorded. The degree of microsphere loading within the hydrogels was obtained by quantifying the ratio of the mass of the microspheres to the overall volume of the hydrogel. The microsphere loading degree was computed using the following equation:

$$\eta = \frac{W_m}{V_m} \quad (4)$$

where  $W_m$  and  $V_m$  are the dropped microsphere mass and mixed solution volume, respectively.<sup>[33]</sup>

#### **2.7.5. Optical microscope observation of microsphere-loaded hydrogels**

The distribution of microspheres within the microsphere-loaded hydrogel was observed using a biological microscope (Mantican 2306, McAuldie Industrial Group Ltd., Hong Kong). Samples from the three groups (ZG40NALO10, ZG35NALO15, ZG30NALO20) were selected and placed in a 24-well plate. Preceding the observation, the 24-well plate containing the GL/NALO hydrogel samples was cleaned and dried with alcohol. The plate was then positioned on the microscope stage and fixed. Adjustments to the sample's positioning were made through the instrument's control handle, until the microsphere-loaded hydrogel's display on the screen was crisp and revealed a uniform and clear distribution.<sup>[34]</sup>

#### **2.7.6. Mechanical property tests of the GL/NALO hydrogels and microsphere-loaded hydrogels**

The hydrogels were shaped into cylindrical forms with dimensions of a 10 mm diameter and a 15 mm thickness to ensure uniformity for testing. For the assessment of compression performance, Instron 5544 (Instron Co., Ltd., USA) a dynamic and static fatigue tester, was employed, utilizing a 5 N sensor, with a needle radius of  $R = 0.5$  mm, and a compression speed of 0.5 mm/min. The compression thickness was set at 2.5 mm. 5 points were randomly selected on each gel block, with one times compressions executed at each of these locations. This process facilitated the capture of consistent displacement

and stress data values. Subsequent analysis was conducted employing Origins software to construct a stress-strain curve.<sup>[35]</sup>

### 2.7.7. Statistical analysis

For each experiment, the significance was assessed through the application of one-way ANOV-A, facilitated by the Statistical Product and Service Solutions (SPSS) software. The results were meticulously evaluated, and a significance level threshold of  $p \leq 0.05$  was established.

## 3. Results and discussion

### 3.1. Characterization of the calcium alginate microspheres

#### 3.1.1. SEM analysis of the microspheres

As depicted in Figures 1A and 1B, SEM imagery provide a clear portrayal of the synthetic calcium alginate gel microspheres. These images show that the morphology of the

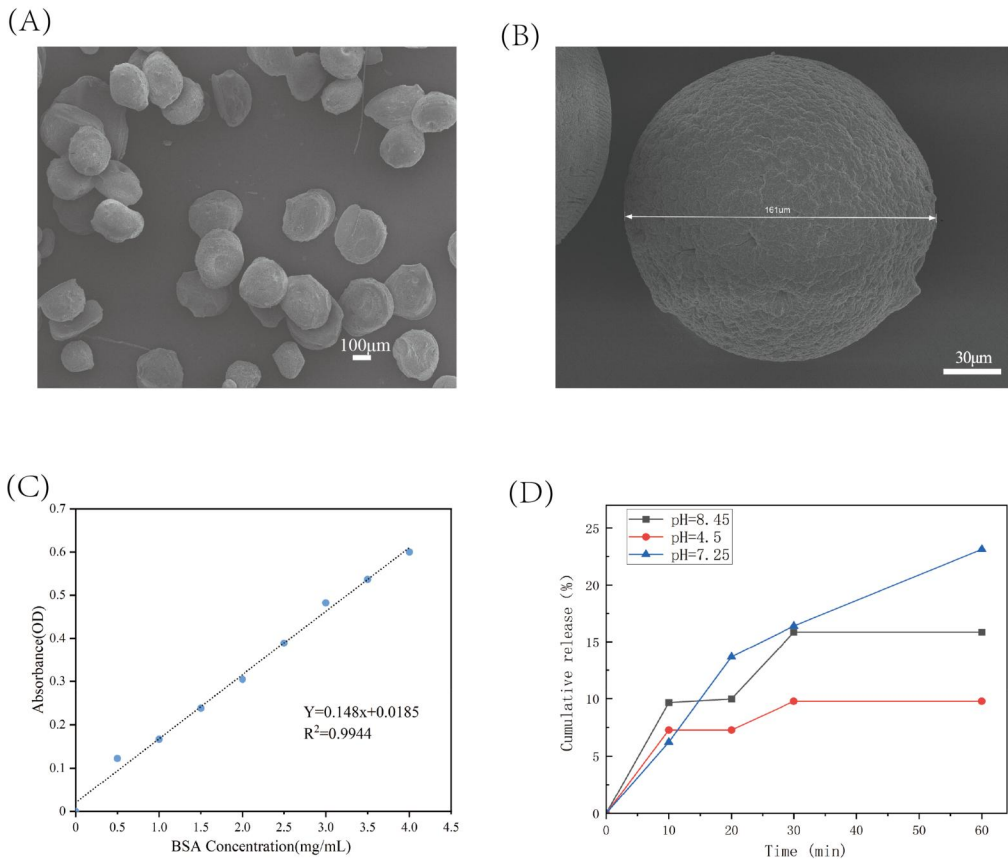


**Figure 1.** Characterization of calcium alginate gel microspheres. (A) SEM image of the microspheres cluster. (B) SEM image of the microspheres surface. (C) Standard curve of bovine serum protein- absorbance in PBS solution. (D) Release curves of BSA-calcium alginate gel microspheres in phosphate buffer solution solutions of various pH.

microspheres presents a complete, smooth, spherical structure with relatively uniform dispersion. Impressively, the microspheres were similar in size and the microspheres' diameters were consistently measured within a range of 150 to 200  $\mu\text{m}$ .

### 3.1.2. Release behavior of BSA from microsphere under different pH conditions

Figure 1C demonstrates the standard curve for the absorbance of BSA in a PBS solution, a crucial reference in understanding the model drug's release behavior. The subsequent analysis of BSA release in phosphate buffers at different pH levels is shown in Figure 1D. This analysis shows a pH-dependent release behavior, with discernible differences across the tested pH of the microspheres. At a neutral pH of 7.25, the release of BSA was observed to be the most rapid, achieving a cumulative release degree of 23.14% within the first hour. Conversely, the acidic environment of pH = 4.5 decelerated the release rate, cumulating in a mere 9.78% release degree at 1 h. The alkaline setting of pH = 8.45 presented a release rate that was intermediate between the neutral and acidic environments, registering a cumulative release degree of 15.86% at 1 h. This typical pH-dependent release behavior underscores a notable contrast in the BSA release rate under neutral and alkaline conditions compared to the sluggish release in the acidic environment. A proposed explanation lies in the alginate's interaction with protons at varying pH levels. In an acidic environment, alginate is likely protonated into an insoluble form, leading to the observed slow diffusion of the BSA.<sup>[36]</sup> Conversely, under neutral conditions, the alginate deprotonation potentially relaxes the microsphere structure, facilitating a more rapid BSA release rate. However, the alkaline conditions may inhibit alginate ionization and induce a certain contraction in the microsphere structure, thereby decelerating the BSA release rate relative to the neutral condition.

## 3.2. Characterization of the GL/NALO hydrogel

### 3.2.1. Hydrogel gel time

Table 1 illustrates the gelation time of the GL/NALO hydrogels at 25 °C, for varying mass ratios of GL and NALO. An intriguing pattern emerges from the results, depicting a proportional increase in gel time of GL/NALO hydrogels corresponding to a decrease in gelatin mass percentage. The underlying mechanism driving this behavior we hypothesize stems from the covalent cross-linking interaction that takes place between the aldehyde group of NALO and the amino group of GL. This complex chemical interaction culminates in the formation of a Schiff base structure, an essential component that connects the molecular chains of sodium alginate and GL together through  $\text{-C=N-}$  bonds.

**Table 1.** Comparison of gel time of GL/NALO with different proportions.

Hydrogel	GL/NALO Concentration ratio	Gel time (min)
G40NALO10	4:1	20
G35NALO15	7:3	25
G30NALO20	3:2	40

### 3.2.2. FTIR spectrometer analysis

Figure 2A shows the FTIR spectra of GL, SA, NALO, and the composite GL/NALO hydrogels. In the study of GL's infrared spectrum, three peaks emerge as pivotal. The

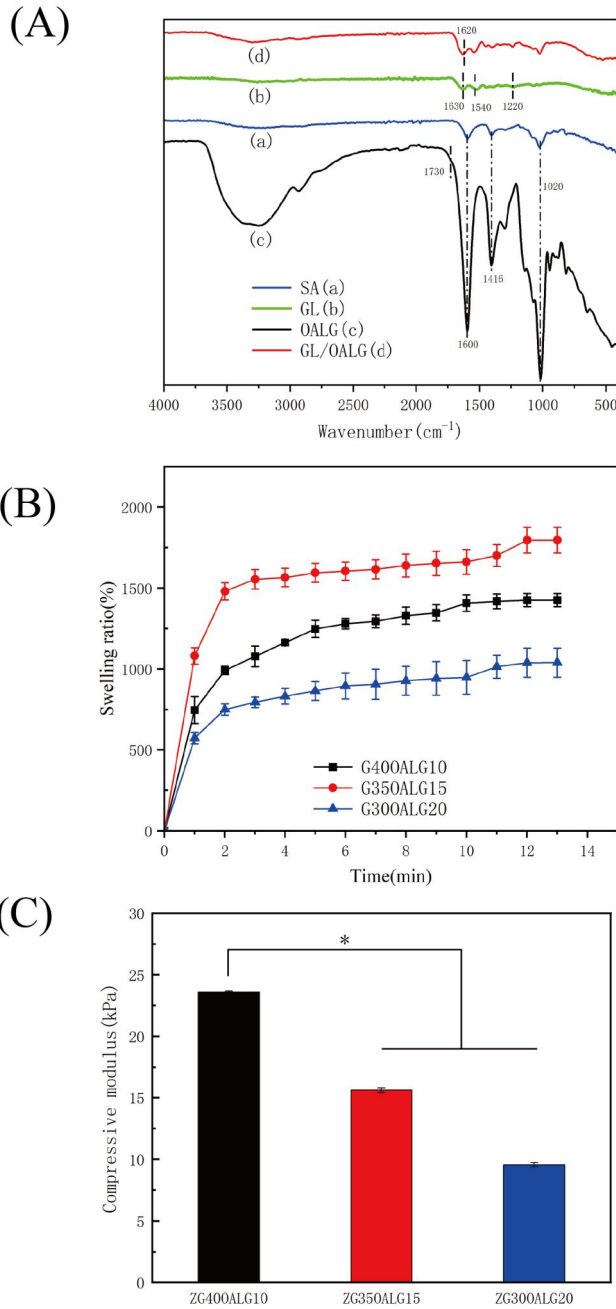


**Figure 2.** Characterization of GL/NALO hydrogel. (A) the infrared spectra of sodium alginate (SA), gelatin(GL), sodium alginate oxide(NALO) and GL/NALO hydrogel. (B) Swelling kinetics curve of GL/NALO with different mass ratios in phosphate buffer solution. (C) Swelling ratio at swelling equilibrium of GL/NALO with different mass ratios in phosphate buffer solution.

stretching vibrations of C=O amide bonds resonate at  $1630\text{ cm}^{-1}$ , the bending vibrations of the N-H amide bonds of the second type surfaces are at  $1540\text{ cm}^{-1}$ , and the stretching vibrations of the third type of amide bonds can be observed at  $1220\text{ cm}^{-1}$ . Simultaneously, sodium alginate exhibits its unique signature, with the symmetric and asymmetric vibrations of the carboxylic acid group C=O bonds manifesting at  $1600$  and  $1416\text{ cm}^{-1}$ , respectively. Additionally, the peak at  $1020\text{ cm}^{-1}$  is attributed to the glycoside C-O bonds' stretching vibrations. A comparison with sodium alginate reveals a novel vibration in the FTIR spectrum of sodium alginate oxide, resonating at  $1730\text{ cm}^{-1}$ , corresponding to the hemiacetal bonds. Intriguingly, the characteristic peak of -CHO at  $1735\text{ cm}^{-1}$  was not detected, possibly obscured by overlapping peaks. The spectrum of the GL/NALO Composite hydrogels introduce a new absorption peak at  $1620\text{ cm}^{-1}$ , denoting a Schiff base structure. This discovery unequivocally verifies the presence of C=N structure within the hydrogels, substantiating the successful formation of the GL/NALO composite hydrogels.

### **3.2.3. Hydrogel swelling**

Figures 2B and 2C show the swelling curves and swelling ratios of the three hydrogels with different proportions, indicating a remarkable capability for water absorption. Each variant of the hydrogel exhibited a swelling equilibrium that exceeded 1000%. The swelling degrees of these hydrogels lay within the range of 1000% and 1800%. Intriguingly, a hydrogel formulated with a 7:3 ratio of GL to NALO demonstrated an unprecedented swelling degree, reaching an astounding value of  $1795 \pm 48\%$ . These hydrogels also manifested excellent deswelling properties. The ability to absorb excessive wound exudate, coupled with an inherent potential to prevent wound infection, show their potential for application in wound healing.

### **3.2.4. Load degree of microspheres in hydrogel**

Figure 3 shows the BSA release profile of the GL/NALO hydrogel when loaded with these microspheres. In our experimental configuration each group of microsphere-loaded hydrogel samples contained 2 mg of microspheres within 4 mL of hydrogel (consisting of 2 mL GL solution and 2 mL NALO solution) volume. This composition yielded a consistent microsphere loading degree of  $0.5\text{ mg/mL}$  across all groups. The experimental variables were strategically confined to the alteration of preparation conditions for the gelatin-oxidized sodium alginate hydrogel. Specifically, modifications were implemented in the mass ratio of GL and NALO by varying their solution concentration.

### **3.2.5. Optical microscope observations of the loaded microsphere hydrogels**

Figures 4A–C present the microscopic images of the three hydrogels samples loaded with microspheres. An astute observation of the visual representations across the three samples shows a remarkable homogeneity in microsphere distribution, which were also found to be similar in particle size and distribution.

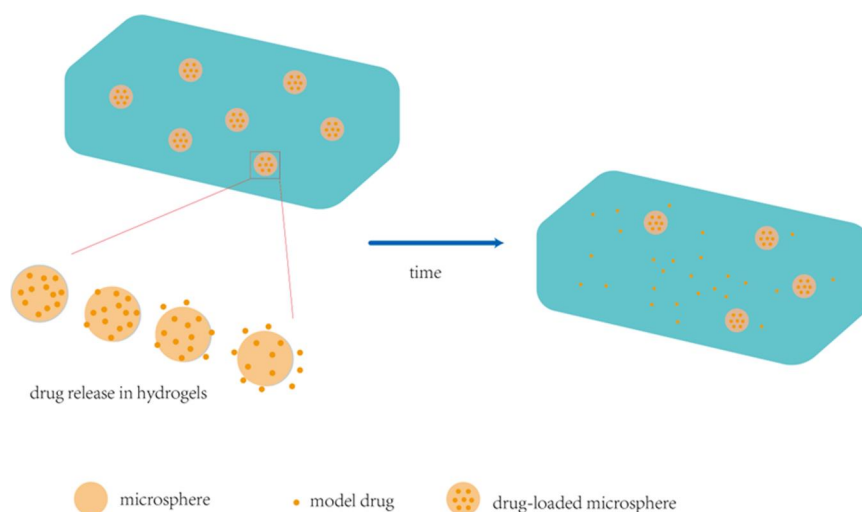


**Figure 3.** Drug release diagram of the GL/NALO hydrogels with loaded microspheres.

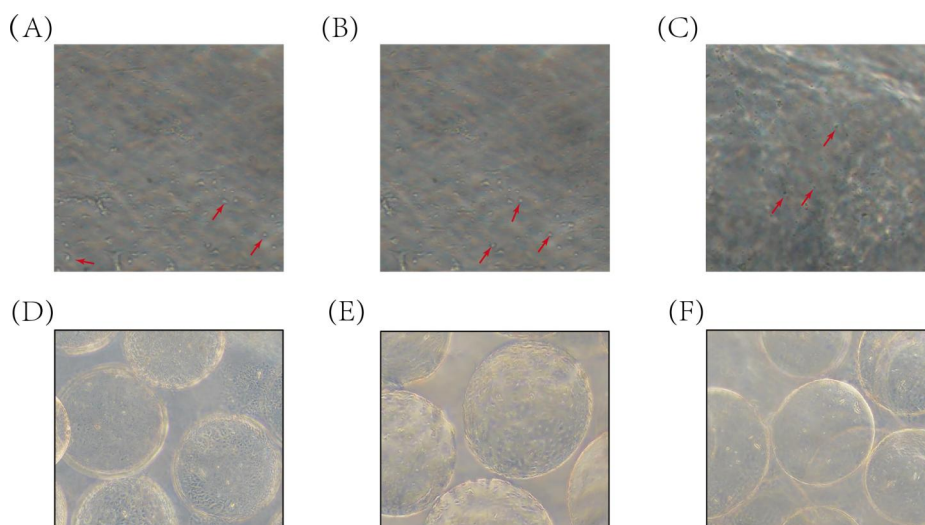


**Figure 4.** Optical microscope image of the microsphere-loaded GL/NALO hydrogels with various mass ratios. (microspheres Indicated by red arrows) (A) microsphere-loaded hydrogel with a GL/NALO mass ratio of 4:1(ZG40NALO10). (B) microsphere-loaded hydrogel with a GL/NALO mass ratio of 7:3(ZG35NALO15). (C) microsphere-loaded hydrogel with a GL/NALO mass ratio of 3:2(ZG30NALO20). (D-F) optical microscope magnified images of the GL/NALO (4:1/7:3/3:2) hydrogels, respectively.

### 3.2.6. Compression properties of the hydrogels and loaded microsphere hydrogels

Figure 5 illustrates the stress-strain curves and elastic moduli for the three GL/NALO hydrogels and their corresponding microsphere-loaded counterparts. An unequivocal pattern emerges, displaying a reduction in the elastic modulus of both hydrogels and

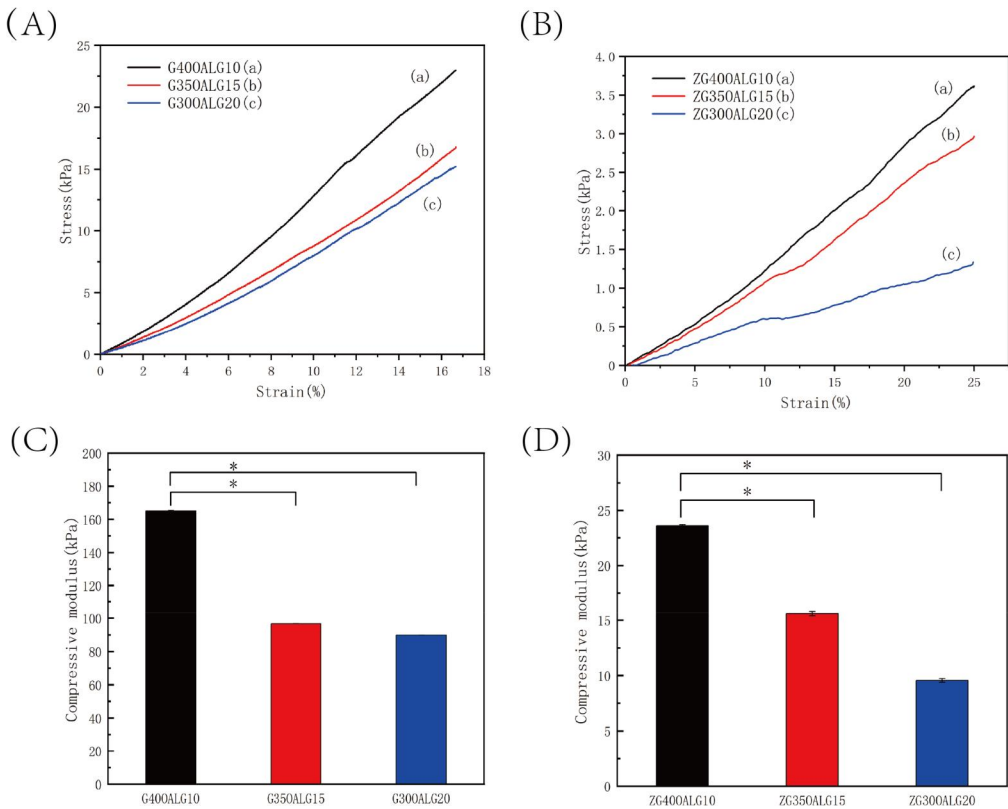


**Figure 5.** Characterization of the mechanical properties of the hydrogels. (A) compression stress–strain curves of the GL/NALO hydrogels. (B) compression stress–strain curves of the microsphere-loaded hydrogels. (C) compressive strength and compressive modulus of the GL/NALO hydrogels. \* $p < 0.05$ . (D) compressive strength and compressive modulus of the microsphere-loaded hydrogels. \* $p < 0.05$ .

BSA-carrying microsphere hydrogels as the concentration of gelatin was increased. Specifically, the elastic modulus descends from  $165.05 \pm 0.58$  kPa for G40NALO10 to  $89.87 \pm 0.19$  kPa for G30NALO20, and from  $23.61 \pm 0.08$  kPa for ZG40NALO10 to  $9.56 \pm 0.16$  kPa for ZG30NALO20. This investigation further shows that the elastic moduli of the BSA-loaded microspheres hydrogels were consistently inferior to those of the GL/NALO hydrogels. The underlying cause for this divergence we attributed to the fact that the addition of microspheres disrupts the cross-linking structure within the GL/NALO hydrogel, and this disruption leads to a reduction in elastic modulus. Worthy of particular note is the microsphere-loaded hydrogel labeled as ZG40NALO10, marked by a gelatin to sodium oxidized alginate mass ratio of 4:1. This specific composite had an elastic modulus closely mirroring human soft tissue, approximately 30 kPa, hence rendering it commendable biomimetic properties. Such findings collectively substantiate that the microspheres incorporation significantly modulates the mechanical properties of the hydrogels, enhancing both their biocompatibility and capacity to replicate biological structures.

## 4. Conclusions

In our research described herein, calcium alginate gel microspheres and microsphere-loaded gelatin/oxyalginate sodium hydrogels were synthesized. Utilizing BSA as a representative model drug, the BSA release behavior of the microspheres was examined, revealing an acute pH responsiveness. This characteristic conferred the microspheres with the capability to adapt their BSA release rate in alignment with fluctuations in environmental pH, attaining its zenith under neutral conditions. The prepared BSA-loaded microspheres hydrogels displayed commendable swelling and mechanical properties, with the swelling properties exceeding tenfold their desiccated weights. Such proficiency endows these hydrogels with the ability to absorb wound exudates, thereby protecting wound surfaces. The elastic modulus of the hydrogels prepared at a GL to NALO ratio of 4:1 approximated that of human skin, bestowing these hydrogels with superior biomimicry. Consequently, the intrinsic properties and performance characteristics observed affirm the potential application of these microsphere-loaded hydrogels in skin dressings.

## Disclosure statement

No potential conflict of interest was reported by the author(s).

## Funding

This work was supported by the National Natural Science Foundation of China (12002232) and the General Project Basic Research Program of Shanxi Province (202103021223100).

## References

- [1] Wang, Q.-Q.; Liu, Y.; Zhang, C.-J.; Zhang, C.; Zhu, P. Alginate/Gelatin Blended Hydrogel Fibers Cross-Linked by Ca<sup>2+</sup> and Oxidized Starch: Preparation and Properties. *Mater. Sci. Eng. C. Mater. Biol. Appl.* **2019**, *99*, 1469–1476. DOI: [10.1016/j.msec.2019.02.091](https://doi.org/10.1016/j.msec.2019.02.091).
- [2] He, Y.; Li, Y.; Sun, Y.; Zhao, S.; Feng, M.; Xu, G.; Zhu, H.; Ji, P.; Mao, H.; He, Y.; Gu, Z. A Double-Network Polysaccharide-Based Composite Hydrogel for Skin Wound Healing. *Carbohydr Polym.* **2021**, *261*, 117870. DOI: [10.1016/j.carbpol.2021.117870](https://doi.org/10.1016/j.carbpol.2021.117870).
- [3] Chen, L.; Tang, Y.; Zhao, K.; Zha, X.; Wei, M.; Tan, Q.; Wu, Z. Sequential Release of Double Drug (Graded Distribution) Loaded Gelatin Microspheres/PMMA Bone Cement. *J. Mater. Chem. B* **2021**, *9*, 508–522. DOI: [10.1039/D0TB01452D](https://doi.org/10.1039/D0TB01452D).
- [4] Yin, X.; Xie, H.; Li, R.; Yan, S.; Yin, H. Regulating Association Strength between Quaternary Ammonium Chitosan and Sodium Alginate via Hydration. *Carbohydr Polym.* **2021**, *255*, 117390. DOI: [10.1016/j.carbpol.2020.117390](https://doi.org/10.1016/j.carbpol.2020.117390).
- [5] Xie, C.-X.; Tian, T.-C.; Yu, S.-T.; Li, L. pH-Sensitive Hydrogel Based on Carboxymethyl Chitosan/Sodium Alginate and Its Application for Drug Delivery: PH-Sensitive Hydrogel Based on Carboxymethyl Chitosan/Sodium Alginate and Its Application for Drug Delivery. *J. Appl. Polym. Sci.* **2019**, *136*, 46911. DOI: [10.1002/app.46911](https://doi.org/10.1002/app.46911).
- [6] Cooke, M. J.; Vulic, K.; Shoichet, M. S. Design of Biomaterials to Enhance Stem Cell Survival When Transplanted into the Damaged Central Nervous System. *Soft Matter* **2010**, *6*, 4988. DOI: [10.1039/c0sm00448k](https://doi.org/10.1039/c0sm00448k).
- [7] Li, Q.; Zhai, W.; Jiang, Q.; Huang, R.; Liu, L.; Dai, J.; Gong, W.; Du, S.; Wu, Q. Curcumin–Piperine Mixtures in Self-Microemulsifying Drug Delivery System for

- Ulcerative Colitis Therapy. *Int. J. Pharm.* **2015**, *490*, 22–31. DOI: [10.1016/j.ijpharm.2015.05.008](https://doi.org/10.1016/j.ijpharm.2015.05.008).
- [8] Leyva-Verduzco, A. A.; Castillo-Ortega, M. M.; Chan-Chan, L. H.; Silva-Campa, E.; Galaz-Méndez, R.; Vera-Graziano, R.; Encinas-Encinas, J. C.; Del Castillo-Castro, T.; Rodríguez-Félix, D. E.; Santacruz-Ortega, H. D. C.; Santos-Sauceda, I. Electrospun Tubes Based on PLA, Gelatin and Genipin in Different Arrangements for Blood Vessel Tissue Engineering. *Polym. Bull* **2020**, *77*, 5985–6003. DOI: [10.1007/s00289-019-03057-7](https://doi.org/10.1007/s00289-019-03057-7).
- [9] Cao, L.; Cao, B.; Lu, C.; Wang, G.; Yu, L.; Ding, J. An Injectable Hydrogel Formed by in Situ Cross-Linking of Glycol Chitosan and Multi-Benzaldehyde Functionalized PEG Analogues for Cartilage Tissue Engineering. *J. Mater. Chem. B.* **2015**, *3*, 1268–1280. DOI: [10.1039/C4TB01705F](https://doi.org/10.1039/C4TB01705F).
- [10] Marroquin-Garcia, R.; Royakkers, J.; Gagliardi, M.; Arreguin-Campos, R.; Cleij, T. J.; Eersels, K.; Van Den Akker, N. M. S.; Molin, D. G. M.; Van Grinsven, B.; Diliën, H. Polyphosphate-Based Hydrogels as Drug-Loaded Wound Dressing: An *in Vitro* Study. *ACS Appl. Polym. Mater.* **2022**, *4*, 2871–2879. DOI: [10.1021/acsapm.1c01533](https://doi.org/10.1021/acsapm.1c01533).
- [11] Thrumurthy, S. G.; Chaudry, M. A.; Thrumurthy, S. S. D.; Mughal, M. Oesophageal Cancer: Risks, Prevention, and Diagnosis. *BMJ* **2019**, *366*, l4373. DOI: [10.1136/bmj.l4373](https://doi.org/10.1136/bmj.l4373).
- [12] Yang, X.; Wang, B.; Peng, D.; Nie, X.; Wang, J.; Yu, C.-Y.; Wei, H. Hyaluronic Acid-Based Injectable Hydrogels for Wound Dressing and Localized Tumor Therapy: A Review. *Adv. NanoBiomed Res.* **2022**, *2*, 2200124. DOI: [10.1002/anbr.202200124](https://doi.org/10.1002/anbr.202200124).
- [13] Zhang, A.; Liu, Y.; Qin, D.; Sun, M.; Wang, T.; Chen, X. Research Status of Self-Healing Hydrogel for Wound Management: A Review. *Int. J. Biol. Macromol.* **2020**, *164*, 2108–2123. DOI: [10.1016/j.ijbiomac.2020.08.109](https://doi.org/10.1016/j.ijbiomac.2020.08.109).
- [14] Fan, J.; Shi, Z.; Lian, M.; Li, H.; Yin, J. Mechanically Strong Graphene Oxide/Sodium Alginate/Polyacrylamide Nanocomposite Hydrogel with Improved Dye Adsorption Capacity. *J. Mater. Chem. A.* **2013**, *1*, 7433. DOI: [10.1039/c3ta10639j](https://doi.org/10.1039/c3ta10639j).
- [15] Wen, Y.; Yu, B.; Zhu, Z.; Yang, Z.; Shao, W. Synthesis of Antibacterial Gelatin/Sodium Alginate Sponges and Their Antibacterial Activity. *Polymers (Basel)* **2020**, *12*, 1926. DOI: [10.3390/polym12091926](https://doi.org/10.3390/polym12091926).
- [16] Bozza, A.; Coates, E. E.; Incitti, T.; Ferlin, K. M.; Messina, A.; Menna, E.; Bozzi, Y.; Fisher, J. P.; Casarosa, S. Neural Differentiation of Pluripotent Cells in 3D Alginate-Based Cultures. *Biomaterials* **2014**, *35*, 4636–4645. DOI: [10.1016/j.biomaterials.2014.02.039](https://doi.org/10.1016/j.biomaterials.2014.02.039).
- [17] Song, Y.; Xu, L.; Xu, L.; Deng, L. Radiation Cross-Linked Gelatin/Sodium Alginate/Carboxymethylcellulose Sodium Hydrogel for the Application as Debridement Glue Paste. *Polym Bull (Berl)* **2022**, *79*, 725–742. DOI: [10.1007/s00289-020-03525-5](https://doi.org/10.1007/s00289-020-03525-5).
- [18] Wang, L.; Zhang, H. J.; Liu, X.; Liu, Y.; Zhu, X.; Liu, X.; You, X. A Physically Cross-Linked Sodium Alginate–Gelatin Hydrogel with High Mechanical Strength. *ACS Appl. Polym. Mater.* **2021**, *3*, 3197–3205. DOI: [10.1021/acsapm.1c00404](https://doi.org/10.1021/acsapm.1c00404).
- [19] Kang, Z.-L.; Wang, T.; Li, Y.; Li, K.; Ma, H. Effect of Sodium Alginate on Physical-Chemical, Protein Conformation and Sensory of Low-Fat Frankfurters. *Meat Sci.* **2020**, *162*, 108043. DOI: [10.1016/j.meatsci.2019.108043](https://doi.org/10.1016/j.meatsci.2019.108043).
- [20] Chen, W.; Tong, Y. W. Mechanisms and Promotion of 3D Neurite Bridging between PHBV Microspheres in a Microsphere–Hydrogel Hybrid Scaffold. *Soft Matter* **2011**, *7*, 11372. DOI: [10.1039/c1sm06473h](https://doi.org/10.1039/c1sm06473h).
- [21] Dragan, E. S. Design and Applications of Interpenetrating Polymer Network Hydrogels. A Review. *Chem. Eng. J.* **2014**, *243*, 572–590. DOI: [10.1016/j.cej.2014.01.065](https://doi.org/10.1016/j.cej.2014.01.065).
- [22] Li, J.; Yang, L.; Zhu, C.; Peng, T.; Huang, D.; Ma, X.; Pan, X.; Wu, C. Release Mechanisms of Bovine Serum Albumin Loaded–PLGA Microspheres Prepared by Ultra-Fine Particle Processing System. *Drug. Drug Deliv. Transl. Res.* **2020**, *10*, 1267–1277. DOI: [10.1007/s13346-020-00774-9](https://doi.org/10.1007/s13346-020-00774-9).
- [23] Wang, W.; Zhou, Z.; Pan, Y.; Liu, W.; Zhou, H.; Liu, Q.; Yan, H.; Zhang, Q. Preparation and Properties of 2, 4-2-Isocyanic Acid Methyl Ester/Poly( $\epsilon$ -Caprolactone)/Diethylene Glycol Hydrogels. *J. Macromol. Sci. Part B. Phys* **2017**, *56*, 245–253. DOI: [10.1080/00222348.2017.1293364](https://doi.org/10.1080/00222348.2017.1293364).

- [24] Wang, Y.; Zhang, S.; Wang, J. Photo-Crosslinkable Hydrogel and Its Biological Applications. *Chin. Chem. Lett.* **2021**, *32*, 1603–1614. DOI: [10.1016/j.ccllet.2020.11.073](https://doi.org/10.1016/j.ccllet.2020.11.073).
- [25] Xiao, Y.; Gu, Y.; Qin, L.; Chen, L.; Chen, X.; Cui, W.; Li, F.; Xiang, N.; He, X. Injectable Thermosensitive Hydrogel-Based Drug Delivery System for Local Cancer Therapy, *Colloids. Colloids Surf B Biointerfaces* **2021**, *200*, 111581. DOI: [10.1016/j.colsurfb.2021.111581](https://doi.org/10.1016/j.colsurfb.2021.111581).
- [26] Amirian, J.; Zeng, Y.; Shekh, M. I.; Sharma, G.; Stadler, F. J.; Song, J.; Du, B.; Zhu, Y. In-Situ Crosslinked Hydrogel Based on Amidated Pectin/Oxidized Chitosan as Potential Wound Dressing for Skin Repairing. *Carbohydr. Polym.* **2021**, *251*, 117005. DOI: [10.1016/j.carbpol.2020.117005](https://doi.org/10.1016/j.carbpol.2020.117005).
- [27] Sarker, B.; Papageorgiou, D. G.; Silva, R.; Zehnder, T.; Gul-E-Noor, F.; Bertmer, M.; Kaschta, J.; Chrissafis, K.; Detsch, R.; Boccaccini, A. R. Fabrication of Alginate–Gelatin Crosslinked Hydrogel Microcapsules and Evaluation of the Microstructure and Physico-Chemical Properties. *J. Mater. Chem. B.* **2014**, *2*, 1470–1482. DOI: [10.1039/c3tb21509a](https://doi.org/10.1039/c3tb21509a).
- [28] Uyen, N. T. T.; Hamid, Z. A. A.; Tram, N. X. T.; Ahmad, N. Fabrication of Alginate Microspheres for Drug Delivery: A Review. *Int. J. Biol. Macromol.* **2020**, *153*, 1035–1046. DOI: [10.1016/j.ijbiomac.2019.10.233](https://doi.org/10.1016/j.ijbiomac.2019.10.233).
- [29] Xi, H.; Yang, L.; Chen, J. Synthesis and Characterization of pH- and Temperature-Sensitive Hydrogels of Poly (Styrene-alt-Maleic Anhydride)-co-Pluronic for Drug Release. *J. Macromol. Sci. Part B. Phys.* **2013**, *52*, 1198–1211. DOI: [10.1080/00222348.2012.755430](https://doi.org/10.1080/00222348.2012.755430).
- [30] Lin, H.; Yin, C.; Mo, A.; Hong, G. Applications of Hydrogel with Special Physical Properties in Bone and Cartilage Regeneration. *Materials* **2021**, *14*, 235. DOI: [10.3390/ma14010235](https://doi.org/10.3390/ma14010235).
- [31] Sarker, B.; Zehnder, T.; Rath, S. N.; Horch, R. E.; Kneser, U.; Detsch, R.; Boccaccini, A. R. Oxidized Alginate-Gelatin Hydrogel: A Favorable Matrix for Growth and Osteogenic Differentiation of Adipose-Derived Stem Cells in 3D. *ACS Biomater. Sci. Eng.* **2017**, *3*, 1730–1737. DOI: [10.1021/acsbiomaterials.7b00188](https://doi.org/10.1021/acsbiomaterials.7b00188).
- [32] Fan, C.; Xu, K.; Huang, Y.; Liu, S.; Wang, T.; Wang, W.; Hu, W.; Liu, L.; Xing, M.; Yang, S. Viscosity and Degradation Controlled Injectable Hydrogel for Esophageal Endoscopic Submucosal Dissection. *Bioact. Mater.* **2021**, *6*, 1150–1162. DOI: [10.1016/j.bioactmat.2020.09.028](https://doi.org/10.1016/j.bioactmat.2020.09.028).
- [33] Reakasame, S.; Boccaccini, A. R. Oxidized Alginate-Based Hydrogels for Tissue Engineering Applications: A Review. *Biomacromolecules* **2018**, *19*, 3–21. DOI: [10.1021/acs.biomac.7b01331](https://doi.org/10.1021/acs.biomac.7b01331).
- [34] Liu, L.; Wu, Q.; Ma, X.; Xiong, D.; Gong, C.; Qian, Z.; Zhao, X.; Wei, Y. Camptothecine Encapsulated Composite Drug Delivery System for Colorectal Peritoneal Carcinomatosis Therapy: Biodegradable Microsphere in Thermosensitive Hydrogel, *Colloids. Colloids Surf B Biointerfaces* **2013**, *106*, 93–101. DOI: [10.1016/j.colsurfb.2013.01.047](https://doi.org/10.1016/j.colsurfb.2013.01.047).
- [35] Jiang, X.; Xiang, N.; Zhang, H.; Sun, Y.; Lin, Z.; Hou, L. Preparation and Characterization of Poly(Vinyl Alcohol)/Sodium Alginate Hydrogel with High Toughness and Electric Conductivity. *Carbohydr Polym* **2018**, *186*, 377–383. DOI: [10.1016/j.carbpol.2018.01.061](https://doi.org/10.1016/j.carbpol.2018.01.061).
- [36] Abbasiliasi, S.; Shun, T. J.; Tengku Ibrahim, T. A.; Ismail, N.; Ariff, A. B.; Mokhtar, N. K.; Mustafa, S. Use of Sodium Alginate in the Preparation of Gelatin-Based Hard Capsule Shells and Their Evaluation *in Vitro*. *RSC Adv.* **2019**, *9*, 16147–16157. DOI: [10.1039/C9RA01791G](https://doi.org/10.1039/C9RA01791G).